CHIN. PHYS. LETT. Vol. 34, No. 11 (2017) 113201

Role of XUV Photons in Atomic High-Order Above-Threshold Ionization Processes in IR+XUV Two-Color Laser Fields *

Kui Zhang(张奎)[1], Min Liu(刘敏)[1], Bing-Bing Wang(王兵兵)[1**], Ying-Chun Guo(郭迎春)[2], Zong-Chao Yan(严宗朝)[3,4,5], Jing Chen(陈京)[6,7**], Xiao-Jun Liu(柳晓军)[4**]

[1]*Laboratory of Optical Physics, Beijing National Laboratory for Condensed Matter Physics, Institute of Physics, Chinese Academy of Sciences, Beijing 100190*

[2]*Department of Physics, East China Normal University, Shanghai 200241*

[3]*Department of Physics, University of New Brunswick, Fredericton, New Brunswick, Canada*

[4]*State Key Laboratory of Magnetic Resonance and Atomic and Molecular Physics, Wuhan Institute of Physics and Mathematics, Chinese Academy of Sciences, Wuhan 430071*

[5]*Center for Cold Atom Physics, Chinese Academy of Sciences, Wuhan 430071*

[6]*HEDPS, Center for Applied Physics and Technology, Peking University, Beijing 100871*

[7]*Institute of Applied Physics and Computational Mathematics, Beijing 100088*

(Received 29 September 2017)

We investigate the above-threshold ionization of an atom in a combined infrared (IR) and extreme ultraviolet (XUV) two-color laser field and focus on the role of XUV field in the high-order above-threshold ionization (HATI) process. It is demonstrated that, in stark contrast to previous studies, the XUV laser may play a significant role in atomic HATI process, and in particular, the XUV laser can accelerate the ionized electron in a quantized way during the collision between the electron and its parent ion. This process cannot be explained by the classical three-step model. Our results indicate that the previously well-established concept that HATI is an elastic recollision process is broken down.

PACS: 32.80.Rm, 42.50.Hz, 32.80.Fb DOI: 10.1088/0256-307X/34/11/113201

With rapid developments of free-electron laser (FEL) technology,[1–3] high-intensity lasers in extreme ultraviolet (XUV) and x-ray regimes have become an important tool for studying light–matter interactions under extreme conditions. The unprecedented properties of these new sources that deliver very intense short wavelength femtosecond pulses have given rise to numerous novel phenomena (for a recent review, see, e.g., Ref. [4]). Recently, various two-color schemes of combining XUV FELs with intense infrared (IR) laser fields have been explored to study atomic photoionization[5–7] and atomic and molecular relaxation processes,[8,9] which provides more insight into the short wavelength intense field atomic dynamics. In particular, for the case of photoionization under two-color (XUV+IR) condition, the most significant characteristic of a photoionization process is represented by a strong modulation of photoelectron spectra by the so-called sideband lines or by above-threshold ionization (ATI) peaks, which are separated from each other by the IR photon energy.[5–7]

This pronounced ATI structure for atoms in an XUV+IR two-color laser field has been well interpreted in the context of laser-assisted photoionization: upon ionization by absorption of the XUV photons, the photoelectron dynamics is completely determined by the IR field and the ATI structure may be understood by interference between electron wavepackets emitted at different periods of the IR laser pulse. Note that in this circumstance, the XUV field was considered as a spectator after the electron becomes free.

In this Letter, we investigate the photoionization dynamics of an atom subjected to a combined intense XUV+IR two-color laser field and focus on the role of the XUV field in the formation of high-order above-threshold ionization (HATI) photoelectron spectrum. Our study relies on a frequency-domain theoretical treatment of laser–matter interaction,[10–13] which has an advantage of separating various ionization channels to facilitate analysis of the roles of the different laser fields, i.e., XUV and IR fields, in the photoelectron dynamics. It is found that the XUV field plays a major role in ionizing the bound electron by a multiphoton absorption (MPA) process; while the IR laser, which can be regarded as a classical field, takes the responsibility for accelerating or decelerating the ionized electron during the collision between the ionized electron and its parent ion in an HATI process. More interestingly and in stark contrast to previous studies, we find that the XUV laser can also play a crucial role in accelerating the ionized electron during

*Supported by the National Natural Science Foundation of China under Grant Nos 11474348, 61275128, 11274050, 11334009 and 11425414, the NSERC of Canada, the Canadian Computing Facilities of SHARCnet and ACEnet, and the National Basic Research Program of China under Grant No 2013CB922200.

**Corresponding author. Email: wbb@aphy.iphy.ac.cn; chen_jing@iapcm.ac.cn; xjliu@wipm.ac.cn

© 2017 Chinese Physical Society and IOP Publishing Ltd

the laser-assisted photoionization process.

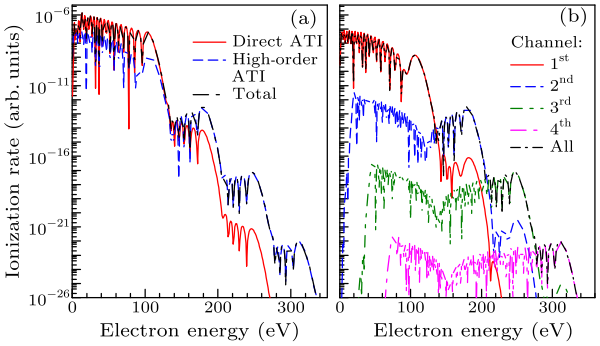


Fig. 1. (Color online) (a) Photoelectron spectra of an atom in an IR+XUV two-color laser field. The ionization threshold of the atom is $I_{\rm p} = 12.1\,{\rm eV}$, the frequencies of the two laser fields are $\omega_1 = 1.165\,{\rm eV}$ and $\omega_2 = 40\omega_1$, and the laser intensities are $I_1 = 1.0\times10^{14}\,{\rm W/cm^2}$ and $I_2 = 1.0\times10^{13}\,{\rm W/cm^2}$, respectively. (b) Photoelectron spectra corresponding to different channels of HATI process.

Based on the frequency-domain theory, the transition matrix of the whole atom-laser system, from the initial state $|\psi_i\rangle$ to the final state $|\psi_{\rm f}\rangle$, can be expressed as (atomic units are used throughout unless otherwise stated)[12]

$$T_{\rm fi} = \langle\psi_{\rm f}|V|\psi_i\rangle + \langle\psi_{\rm f}|U(\boldsymbol{r})\frac{1}{E_{\rm f}-H+i\varepsilon}V|\psi_i\rangle, \quad (1)$$

where $H = H_0 + U(\boldsymbol{r}) + V$ is the Hamiltonian of the system, with $H_0 = (-i\nabla)^2/2 + \omega_1 N_1 + \omega_2 N_2$ being the energy operator of a free electron–laser system, N_1 and N_2 are the photon number operators of the two fields with frequencies ω_1 and ω_2, respectively, $U(\boldsymbol{r})$ is the atomic binding potential, V is the electron–laser interaction operator, and $E_{\rm f}$ is the eigenvalue of the final state $|\psi_{\rm f}\rangle$. The first term in Eq. (1) corresponds to the direct ATI process, while the second term corresponds to the HATI process. Particularly, the transition matrix element of an HATI process in a combined IR+XUV two-color laser field can be expressed as

$$\begin{aligned} T_{\rm r} = {} & \frac{-i}{8\pi^2 V_{\rm e}^{1/2}}\sum_{q_2}\sum_{q_1}\sum_{s_1 s_2}[(u_{\rm p,1}-s_1)\omega_1 \\ & + (u_{\rm p,2}-s_2)\omega_2]|\boldsymbol{p}_{\rm m}| \\ & \times \int U_{\boldsymbol{p}_{\rm f}\boldsymbol{p}_{\rm m}}\Phi_i(\boldsymbol{p}_{\rm m})J_{q_1-s_1}(\zeta_{1{\rm m}}-\zeta_{1{\rm f}})\mathcal{J}_{s_1,s_2}(\zeta_{\rm m}) \\ & \times J_{q_2-s_2}(\zeta_{2{\rm m}}-\zeta_{2{\rm f}})\sin\theta_{\boldsymbol{p}_{\rm m}}d\theta_{\boldsymbol{p}_{\rm m}}d\varphi_{\boldsymbol{p}_{\rm m}}, \end{aligned} \quad (2)$$

where s_1 (s_2) is the IR (XUV) photon number that the electron absorbs in the first step, $|\boldsymbol{p}_{\rm m}| = \sqrt{2[(s_1-u_{\rm p,1})\omega_1 + (s_2-u_{\rm p,2})\omega_2 - I_{\rm p}]}$ is the absolute value of the electron momentum before collision, $U_{\boldsymbol{p}_{\rm f}\boldsymbol{p}_{\rm m}} = \int d\boldsymbol{r}e^{-i\boldsymbol{p}_{\rm f}\cdot\boldsymbol{r}}U(\boldsymbol{r})e^{i\boldsymbol{p}_{\rm m}\cdot\boldsymbol{r}}$ with $U(\boldsymbol{r})$ being replaced by a short-range potential $U(\boldsymbol{r}) = -\hat{\epsilon}\exp(-r)/r$, $\zeta_{jm} = 2\sqrt{u_{{\rm p},j}/\omega_j}|\boldsymbol{p}_{\rm m}\cdot\hat{\boldsymbol{\epsilon}}_j|$ and $\zeta_{j{\rm f}} = 2\sqrt{u_{{\rm p},j}/\omega_j}|\boldsymbol{p}_{\rm f}\cdot\hat{\boldsymbol{\epsilon}}_j|$ with $j = 1, 2$, $\mathcal{J}_{s_1,s_2}(\zeta_{\rm m})$ is a generalized Bessel function,[14] and $\theta_{p_{\rm m}}$ is the angle between $\boldsymbol{p}_{\rm m}$ and $\boldsymbol{p}_{\rm f}$ with $\boldsymbol{p}_{\rm m}$ and $\boldsymbol{p}_{\rm f}$ being the momenta of the electron before and after the collision, respectively.

Figure 1(a) presents the total ATI spectrum of an atom in an IR+XUV two-color laser field with the polarizations of both lasers along the same direction. The frequencies of the two lasers are $\omega_1 = 1.165\,{\rm eV}$ and $\omega_2 = 40\omega_1$, and their intensities are $I_1 = 1.0\times10^{14}\,{\rm W/cm^2}$ and $I_2 = 1.0\times10^{13}\,{\rm W/cm^2}$, respectively. It can be seen that both the direct ATI and HATI spectra show a multi-plateau structure with identical cutoffs, which is quite different from the case of the monochromatic IR laser, where the cutoffs of the direct ATI and HATI spectra are about $2U_{\rm p,1}$ and $10U_{\rm p,1}$, respectively. Moreover, one can find that the direct ATI process dominates the first plateau, while the HATI dominates higher-order plateaus. In the following we will focus on the HATI and aim to uncover the role of the XUV laser in the HATI photoelectron dynamics.

To facilitate the analysis, we first distinguish different quantum channels in the HATI by defining the q_2th channel as the one where the atom absorbs q_2 XUV photons in the whole ionization process. In Fig. 1(b), the first four channels are shown. It can be seen that the total number of the XUV photons absorbed by the ionized electron determines the height of the corresponding plateau, and interestingly, a pronounced dip structure is present in the intermediate regime of the spectra for the higher order channels (i.e., $q_2 > 1$), which will be discussed in the following.

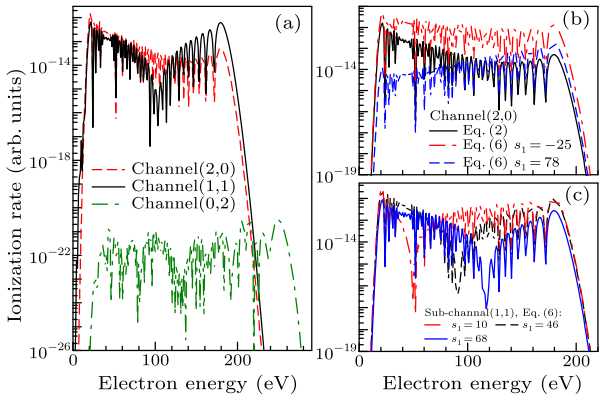


Fig. 2. (Color online) The HATI spectra for the second channel (a), sub-channels $(2,0)$ (b) and $(1,1)$ (c).

It has been shown that an HATI process can be regarded as an ATI followed by a laser-assisted collision (LAC),[12] and for both steps the XUV photons may be absorbed. In the following we will illustrate that, in stark contrast to previous studies, the XUV laser could play a significant role in photoelectron dynamics after the electron becomes free, giving rise to nontrivial features in HATI spectra. To illustrate this effect, we further define the sub-channels in the q_2th channel as $(s_2, q_2 - s_2)$, where s_2 and $q_2 - s_2$

are the XUV photon numbers absorbed in the ATI and LAC steps, respectively. Taking the second HATI channel ($q_2 = 2$) as an example, Fig. 2(a) shows the HATI spectra for three sub-channels $(2,0)$, $(1,1)$ and $(0,2)$. One can see that the ionization amplitude from the sub-channel $(0,2)$ is lower than that of the sub-channels $(2,0)$ and $(1,1)$ by about 10 orders of magnitude, which is because absorbing XUV photons in the ATI step can effectively increase the HATI probability. On the other hand, the sub-channels $(1,1)$ and $(2,0)$ have a comparable ionization strength and both contribute to the HATI process significantly. Moreover, while both spectra of the sub-channels $(2,0)$ and $(1,1)$ have a similar cutoff position, the contribution to the cutoff region from $(1,1)$ channel overwhelms that from $(2,0)$. Also note that the sub-channel $(1,1)$ presents an obvious dip at about the middle of its spectrum which is the source of the dip in the spectrum of the second channel (see Fig. 1(b)). It is worth mentioning that the sub-channel $(1,1)$ corresponds to the absorption of one XUV photon by the ionized electron in the LAC step, which is a quantum process beyond the classical recollision perspective.

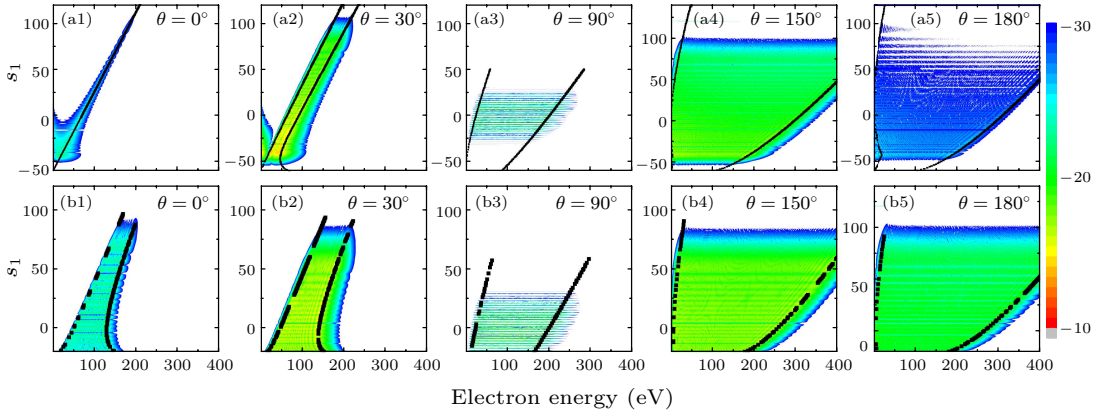


Fig. 3. (Color online) The HATI spectrum as a function of s_1 for sub-sub-channel $(2,0|s_1)$ ((a1)–(a5)) and $(1,1|s_1)$ ((b1)–(b5)). The incoming direction of the collision electron $\theta_{\boldsymbol{p}_\mathrm{m}} = 0$ for (a1) and (b1), 30° for (a2) and (b2), 90° for (a3) and (b3), 150° for (a4) and (b4), and 180° for (a5) and (b5), respectively.

To understand the significant role of the XUV laser in the HATI process and the closely related spectral structures of the sub-channel $(1,1)$, we further define the sub-sub-channel (SSC) $(s_2, q_2 - s_2|s_1)$ within each sub-channel $(s_2, q_2 - s_2)$, where the electron absorbs s_1 IR photons and s_2 XUV photons in the ATI step, while it absorbs $q_2 - s_2$ XUV photons in the LAC step. Figure 3 presents the HATI spectra of SSC $(2,0|s_1)$ (Figs. 3(a1)–3(a5)) and $(1,1|s_1)$ (Figs. 3(b1)–3(b5)) for different incoming directions of the electron before it collides with the ion, i.e., $\theta_{\boldsymbol{p}_\mathrm{m}} = 0$ (Figs. 3(a1) and 3(b1)), 30° (Figs. 3(a2) and 3(b2)), 90° (Figs. 3(a3) and 3(b3)), 150° (Figs. 3(a4) and 3(b4)) and 180° (Figs. 3(a5) and 3(b5)). We may find that the spectrum for a forward collision, i.e., $\theta_{\boldsymbol{p}_\mathrm{m}} < 90°$, changes from a very narrow band to a wide band as the incoming angle $\theta_{\boldsymbol{p}_\mathrm{m}}$ increases; while the spectrum for the backward collision, i.e., $\theta_{\boldsymbol{p}_\mathrm{m}} > 90°$, always presents a relatively uniform wide band with a certain width. Moreover, the low-energy part of the HATI spectrum for both SSCs is determined by the forward collision, while the spectrum cutoff is determined by the backward collision.

To explain the band structure of the spectra shown in Fig. 3 and to further elaborate the role of the XUV field in HATI process, we now treat the IR laser field as a classical field and use the saddle-point approximation in the LAC process for SSC $(s_2, q_2 - s_2|s_1)$. Let us consider an electron in a classical IR laser field with potential $\boldsymbol{A}_\mathrm{cl}(t) = \hat{\boldsymbol{\epsilon}}_1 \mathcal{E}_1/\omega_1 \cos(\omega_1 t)$, and the corresponding classical action is $S_\mathrm{cl}(t, \boldsymbol{p}) = \frac{1}{2}\int dt[\boldsymbol{p} + \boldsymbol{A}_\mathrm{cl}(t)]^2$. By applying the saddle-point approximation, we obtain

$$\frac{[\boldsymbol{p}_\mathrm{f} + \boldsymbol{A}_\mathrm{cl}(t_\mu)]^2}{2} = \frac{[\boldsymbol{p}_\mathrm{m} + \boldsymbol{A}_\mathrm{cl}(t_\mu)]^2}{2} + (q_2 - s_2)\omega_2. \quad (3)$$

Using Eq. (3), the minimal and maximal values of the final kinetic energy can be obtained as

$$E_\mathrm{f}^\mathrm{min} = [\sqrt{\Delta E' + E_\mathrm{L} + 2\sqrt{E_\mathrm{L}\Delta E}\cos(\theta_{\boldsymbol{p}_\mathrm{m}})} - \sqrt{E_\mathrm{L}}]^2, \quad (4)$$

$$E_\mathrm{f}^\mathrm{max} = [\sqrt{\Delta E' + E_\mathrm{L} - 2\sqrt{E_\mathrm{L}\Delta E}\cos(\theta_{\boldsymbol{p}_\mathrm{m}})} + \sqrt{E_\mathrm{L}}]^2, \quad (5)$$

where $\Delta E' = s_1\omega_1 + q_2\omega_2 - U_{\mathrm{p},1} - U_{\mathrm{p},2} - I_\mathrm{p}$, $\Delta E = \Delta E' - (q_2 - s_2)\omega_2$, and $E_\mathrm{L} = 2U_{\mathrm{p},1}$. The minimal and maximal values of the spectrum given by the above two formulas are shown by the black dashed curves in Fig. 3, which agree well with the numerical calculation. In particular, for SSC $(2,0|s_1)$ we have $\Delta E' = \Delta E$, hence for $\theta_{\boldsymbol{p}_\mathrm{m}} = 0$, Eqs. (4) and (5) give $E_\mathrm{f} = E_{\boldsymbol{p}_\mathrm{m}}$, which indicates that the electron keeps its energy after the collision. The spectrum thus shows a very narrow band in Fig. 3(a1). For $\theta_{\boldsymbol{p}_\mathrm{m}} \neq 0$, we have $E_\mathrm{min} \neq E_\mathrm{max}$, hence the electron can exchange

photons during the collision with the ion and presents a relatively uniform band in the photoelectron spectrum. In contrast, for the SSC $(1,1|s_1)$ the electron absorbs one XUV photon during the collision and thus $\Delta E' \neq \Delta E$. As a consequence, the spectrum shows a band structure even when $\theta_{\boldsymbol{p}_\mathrm{m}} = 0$, indicating that the electron always exchanges photons with the IR laser during the collision process. The most obvious difference for the spectra of SSCs $(2,0|s_1)$ and $(1,1|s_1)$ occurs at $\theta_{\boldsymbol{p}_\mathrm{m}} = 180°$, corresponding to the so-called backward collision as shown in Figs. 3(a5) and 3(b5), where the amplitude of the spectrum for SSC $(1,1|s_1)$ is much larger than that for $(2,0|s_1)$. This is because the electron absorbs two XUV photons in the first step for SSC $(2,0|s_1)$, while it absorbs only one XUV photon for $(1,1|s_1)$. Hence, in general, the momentum of the electron in SSC $(2,0|s_1)$ before collision is larger than that in $(1,1|s_1)$. As is well-known, the probability of the backward collision decreases with the incoming momentum of the particle, hence the strength of the spectrum for $(2,0|s_1)$ is smaller than that for $(1,1|s_1)$. Since the backward collision mainly contributes to the spectrum in the high-energy region, the high energy part of the spectrum of the $(1,1|s_1)$ channel is higher than that of the $(2,0|s_1)$ channel (see Fig. 2(a)), indicating that the process in which the XUV photon is absorbed during the collision plays a dominant role in the HATI spectrum.

We now aim to understand the specific structure (e.g., the dip) and cutoff values in the spectra for sub-channels $(2,0)$ and $(1,1)$. For the present laser condition, the formula of the transition matrix for sub-channel $(s2, q2-s2)$ can be simplified to

$$T_\mathrm{r}^{(s_2,q_2-s_2)} \approx -i\pi^{-2}/8V_\mathrm{e}^{-1/2}[(u_{\mathrm{p},1}-\widetilde{s}_1)\omega_1 + (u_{\mathrm{p},2}-s_2)\omega_2]|\boldsymbol{p}_\mathrm{m}| \int U_{\boldsymbol{p}_\mathrm{f}\boldsymbol{p}_\mathrm{m}}\Phi_i(\boldsymbol{p}_\mathrm{m})J_{q_2-s_2} \times (\zeta_{2\mathrm{m}}-\zeta_{2\mathrm{f}})J_{-s_2}(\zeta_{2\mathrm{m}})J_{-q_1}(\zeta_{1\mathrm{f}},\zeta_3)d^3\boldsymbol{p}_\mathrm{m}, \quad (6)$$

where $J_{-q_1}(\zeta_{1\mathrm{f}},\zeta_3) = \sum_{q_3} J_{-q_1+2q_3}(\zeta_{1\mathrm{f}})J_{-q_3}(\zeta_3)$. Figures 2(b) and 2(c) present the spectra obtained by Eq. (6) for sub-channel $(2,0)$ with $\widetilde{s}_1 = -25$ and 87, and for sub-channel $(1,1)$ with $\widetilde{s}_1 = 10$, 46 and 68, respectively. It is found that the main spectral features in Fig. 2(a), and in particular, the dip structure for the sub-channel $(1,1)$, can be reproduced by the results obtained by Eq. (6). Furthermore, from Eq. (6), it can be found that the dip structure for the sub-channel $(1,1)$ comes from the fact that the Bessel function $J_{q_2-s_2}(\zeta_{2\mathrm{m}}-\zeta_{2\mathrm{f}}) = 0$ for $\boldsymbol{p}_\mathrm{f} = \boldsymbol{p}_\mathrm{m}$. Therefore, the formation of the dip structure may be understood as follows: if there is no IR laser field, since the electron absorbs one XUV photon in the LAC process, the final momentum $\boldsymbol{p}_\mathrm{f}$ cannot be equal to the intermediate momentum $\boldsymbol{p}_\mathrm{m}$, hence the probability of HATI for $\boldsymbol{p}_\mathrm{f} = \boldsymbol{p}_\mathrm{m}$ will be zero. However, because of the existence of the IR laser field, which now can be regarded as a classical field, the electron can be accelerated or decelerated by the IR laser field in the LAC process. Therefore, the probability of the HATI is no longer zero but reaches a minimum as far as $\boldsymbol{p}_\mathrm{f} = \boldsymbol{p}_\mathrm{m}$ (see Figs. 2(c)). Moreover, the final position of the dip in the total HATI spectrum is determined by the average effect of contributions from all SSCs.

We then turn to the cutoff in the sub-channel spectra. Similarly, using the saddle-point approximation in Eq. (6), the cutoff formula for sub-channel (s_2, q_2-s_2) can be written as

$$E_\mathrm{max} = (\sqrt{q_2\omega_2 - I_\mathrm{p}} + \sqrt{2U_{\mathrm{p},1}})^2. \quad (7)$$

We notice that this formula only depends on the total number of the XUV photons q_2 and exhibits an independence on s_2. Consequently, the sub-channels $(2,0)$ and $(1,1)$ possess an identical cutoff value in their spectra, and therefore, the cutoff value of the second channel is also determined by Eq. (7). In general, the cutoff values of all channels in HATI spectra obey the above cutoff formula, which is the same as the direct ATI spectrum.[14] Therefore, these results explain why the corresponding plateaus in the direct ATI and HATI spectra have the same cutoff values.

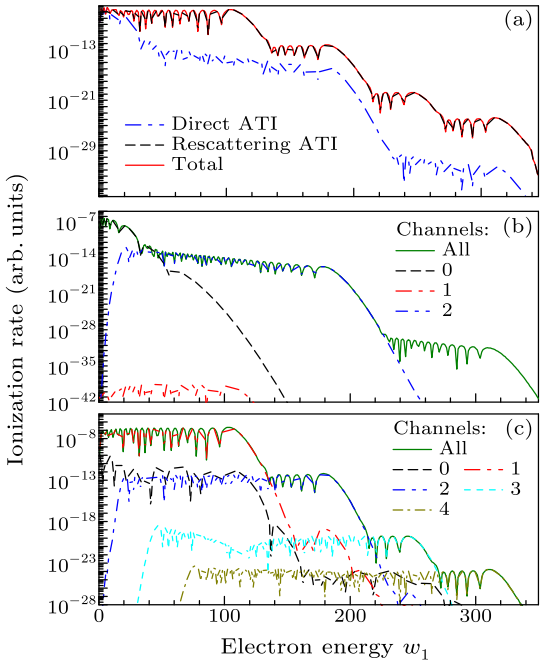


Fig. 4. (Color online) (a) The spectrum of photoelectrons that are emitted along the polarization direction of the IR laser. Note that the polarizations of IR and XUV laser fields are perpendicular to each other; and the spectra of various channels for the direct ATI (b) and HATI (c) processes, respectively.

Since the direct ATI and HATI spectra have similar step-like structure with the same cutoff values, then one may ask how to identify these two processes in the spectrum. We find that it can be achieved by setting the polarization directions of the two lasers

to be perpendicular with each other and by detecting the photoelectrons emitted along the polarization direction of the IR laser.

Figure 4(a) presents the total spectrum. Comparing Fig. 4(a) with Fig. 1(a), one finds that the spectrum is now dominated by the HATI process even in the first plateau except in the very low energy region. This can be explained by analyzing the various channel contributions for both spectra as shown in Fig. 4 for ATI and HATI. One sees in Fig. 4(b) that the spectrum is dominated by the even-number ATI channels, where the electron can only absorb an even number of XUV photons. This phenomenon has been recently observed in the ATI spectrum in a monochromatic IR laser field by Korneev *et al.*,[15] and was explained in terms of the interference between the long and short quantum orbits. In contrast, Fig. 4(c) shows that, for the HATI spectrum, the electron can absorb both odd and even number XUV photons, which can be understood as follows: upon ionization by absorption of any number of XUV and IR photons in the first step, the electron will further absorb more IR and XUV photons in the second (LAC) step and runs along the polarization direction of the IR laser. The additional absorption of XUV photons in the LAC results in breakdown of the even-number photon-absorption rule for the HATI process, giving rise to the dominance of HATI over ATI contribution in the spectrum. This provides a possibility of experimental access to the HATI process.

In conclusion, we have investigated the HATI process of an atom in a combined IR and XUV two-color laser field where the HATI spectrum presents a multiplateau structure. By analyzing ionization channels, we find that, in the HATI spectrum, the forward collision of the ionized electron determines the structure of the low-energy part of the plateau, while the backward collision determines the cutoff of the plateau. Moreover, the XUV photon can also be absorbed during the collision between the ionized electron and its ionic core and more interestingly, this process plays a dominant role in the high-energy region of the HATI spectrum.

We thank W. Becker and the members of the SFAMP club for helpful discussions and suggestions.

References

[1] Ackermann W et al 2007 *Nat. Photon.* **1** 336
[2] Shintake T et al 2008 *Nat. Photon.* **2** 555
[3] Emma P et al 2010 *Nat. Photon.* **4** 641
[4] Feldhaus J et al 2013 *J. Phys.* B **46** 164002
[5] Meyer M et al 2010 *J. Phys.* B **43** 194006
[6] Radcliffe P et al 2012 *New J. Phys.* **14** 043008
[7] Duesterer S et al 2013 *J. Phys.* B **46** 164026
[8] Mazza T et al 2012 *J. Phys.* B **45** 141001
[9] Krikunova M et al 2011 *J. Chem. Phys.* **134** 024313
[10] Guo D S et al 1988 *J. Phys.* A **21** 4577
Guo D S et al 1989 *Phys. Rev.* A **40** 4997
Guo D S and Drake G W F 1992 *J. Phys.* A **25** 3383
[11] Gao L, Li X, Fu P, Freeman R R and Guo D S 2000 *Phys. Rev.* A **61** 063407
[12] Wang B, Gao L, Li X, Guo D S and Fu P 2007 *Phys. Rev.* A **75** 063419
[13] Wang B, Guo Y, Chen J, Yan Z C and Fu P 2012 *Phys. Rev.* A **85** 023402
[14] Zhang K, Chen J, Hao X L, Fu P, Yan Z C and Wang B 2013 *Phys. Rev.* A **88** 043435
[15] Korneev P A, Popruzhenko S V, Goreslavski S P, Yan T M, Bauer D, Becker W, Kübel M, Kling M F, Rödel C, Wünsche M and Paulus G G 2012 *Phys. Rev. Lett.* **108** 223601